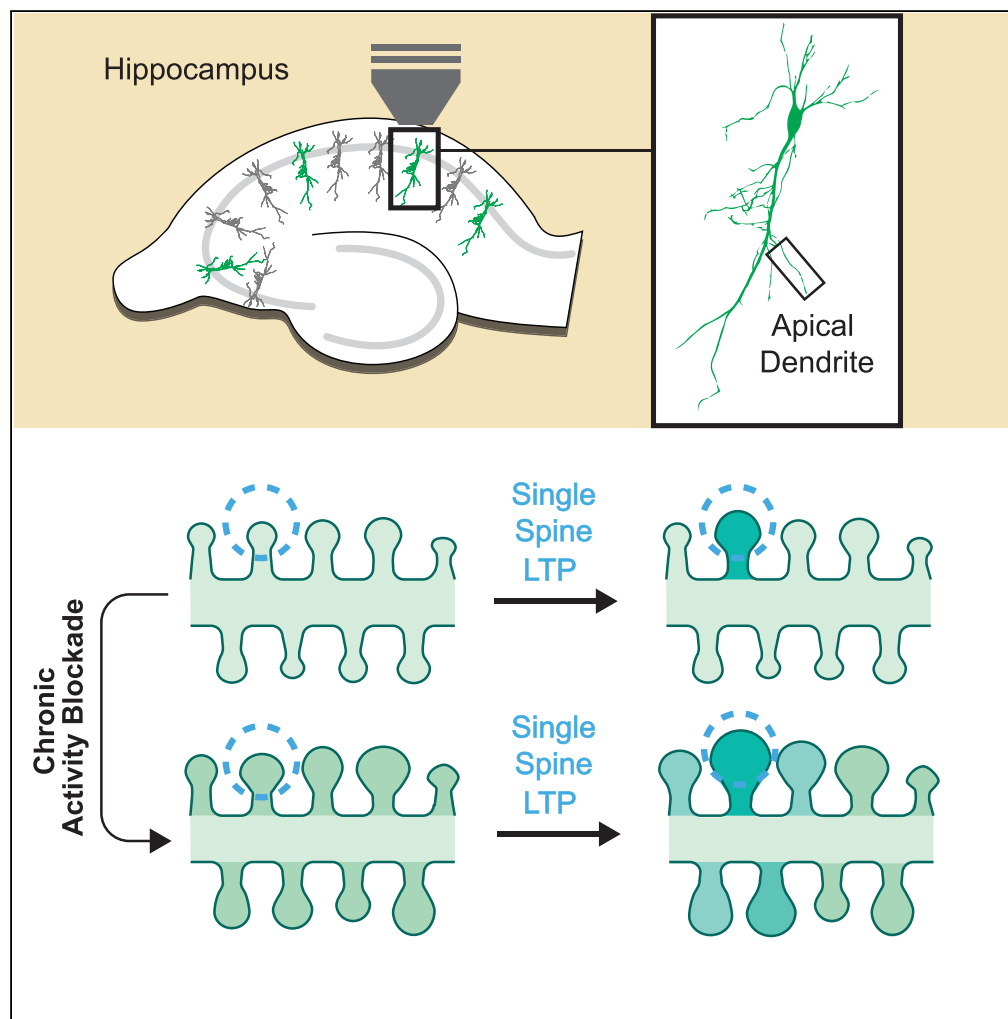


Article

Homeostatic Plasticity Scales Dendritic Spine Volumes and Changes the Threshold and Specificity of Hebbian Plasticity



Anna Felicity Hobbiss, Yazmin Ramiro-Cortés, Inbal Israely

ii2176@columbia.edu

HIGHLIGHTS

Chronic activity blockade leads to enlarged hippocampal spines and structural scaling

Homeostatic plasticity affects subsequent Hebbian plasticity according to size of spines

Neighbors also grow after potentiation of single spines, compromising input specificity

Hobbiss et al., iScience 8, 161–174
October 26, 2018 © 2018 The Authors.
<https://doi.org/10.1016/j.isci.2018.09.015>



Article

Homeostatic Plasticity Scales Dendritic Spine Volumes and Changes the Threshold and Specificity of Hebbian Plasticity

Anna Felicity Hobbiss,¹ Yazmin Ramiro-Cortés,^{1,2} and Inbal Israely^{1,3,4,*}

SUMMARY

Information is encoded in neural networks through changes in synaptic weights. Synaptic learning rules involve a combination of rapid Hebbian plasticity and slower homeostatic synaptic plasticity that regulates neuronal activity through global synaptic scaling. Hebbian and homeostatic plasticity have been extensively investigated, whereas much less is known about their interaction. Here we investigated structural and functional consequences of homeostatic plasticity at dendritic spines of mouse hippocampal neurons. We found that prolonged activity blockade induced spine growth, paralleling synaptic strength increases. Following activity blockade, glutamate uncaging-mediated stimulation at single spines led to size-dependent structural potentiation: smaller spines underwent robust growth, whereas larger spines remained unchanged. Moreover, spines near the stimulated spine exhibited volume changes following homeostatic plasticity, indicating that there was a breakdown of input specificity following homeostatic plasticity. Overall, these findings demonstrate that Hebbian and homeostatic plasticity interact to shape neural connectivity through non-uniform structural plasticity at inputs.

INTRODUCTION

Hebbian synaptic plasticity, widely regarded as the leading biological mechanism for information storage, involves activity-dependent changes in synaptic connectivity (Malenka and Bear, 2004). Notably, these changes have a physical component and excitatory postsynaptic current is highly correlated with dendritic spine volume. However, left unchecked activity would lead to a positive feedback loop in which changes in synaptic weight are further reinforced by future events. This has been proposed to result in loss of functionality of the system, by either driving synapses toward saturation, or through silencing the population. How neurons maintain stability in the face of destabilizing cellular and circuit events has been a long-standing question. One method neurons employ to resolve this is homeostatic synaptic plasticity (HSP), a feedback mechanism through which a population of synapses can be maintained to function within optimal bounds. During HSP, a decrease in global activity drives a counteracting scalar increase in synaptic strengths to bring the network into an optimal functioning range, and conversely, network activity increases will promote synaptic weakening (Turrigiano, 2011). This scaling is instantiated in part by AMPA receptor trafficking to and from the postsynaptic density, as well as through presynaptic changes that modify neurotransmitter release, leading to concomitant changes in synaptic strength (Murthy et al., 2001; O'Brien et al., 1998). HSP has been observed both *in vitro* and *in vivo* (Desai et al., 2002; Turrigiano et al., 1998), supporting a fundamental role for this mechanism in the proper functioning of the neural system.

Increasing evidence points to structural correlates of homeostatic plasticity (Barnes et al., 2017; Keck et al., 2013; Kirov and Harris, 1999). Although it is well established that HSP modulates synaptic function, it is currently unknown how this process dynamically regulates spine structural changes and how such alterations affect the encoding of subsequent activity. Specifically, how HSP affects the induction and longevity of subsequent forms of Hebbian plasticity at individual inputs is yet to be determined. In this study, we examine how the induction of HSP affects the structure and function of hippocampal pyramidal neuron synapses and what are the consequences of these changes for future Hebbian plasticity. We find that the induction of HSP, due to chronic activity blockade, leads to an initial supralinear increase in the size of spines that over time becomes linear, thus producing structural scaling that matches the functional scaling of synapses. Through precise 2-photon-mediated glutamate uncaging, we further investigate how these homeostatic functional and structural plasticity changes affect the ability of individual inputs to undergo subsequent plasticity. We demonstrate that after HSP, spines express increased longevity of

¹Champalimaud Centre for the Unknown, Lisbon 1400-038, Portugal

²Instituto de Fisiología Celular, Universidad Nacional Autónoma de México, Ciudad Universitaria, Circuito exterior s/n, Ciudad de México 04510, México

³Department of Pathology and Cell Biology in the Taub Institute for Research on Alzheimer's Disease and the Aging Brain, Department of Neuroscience, College of Physicians & Surgeons, Columbia University, New York, NY 10032, USA

⁴Lead Contact

*Correspondence:
ii2176@columbia.edu

<https://doi.org/10.1016/j.isci.2018.09.015>



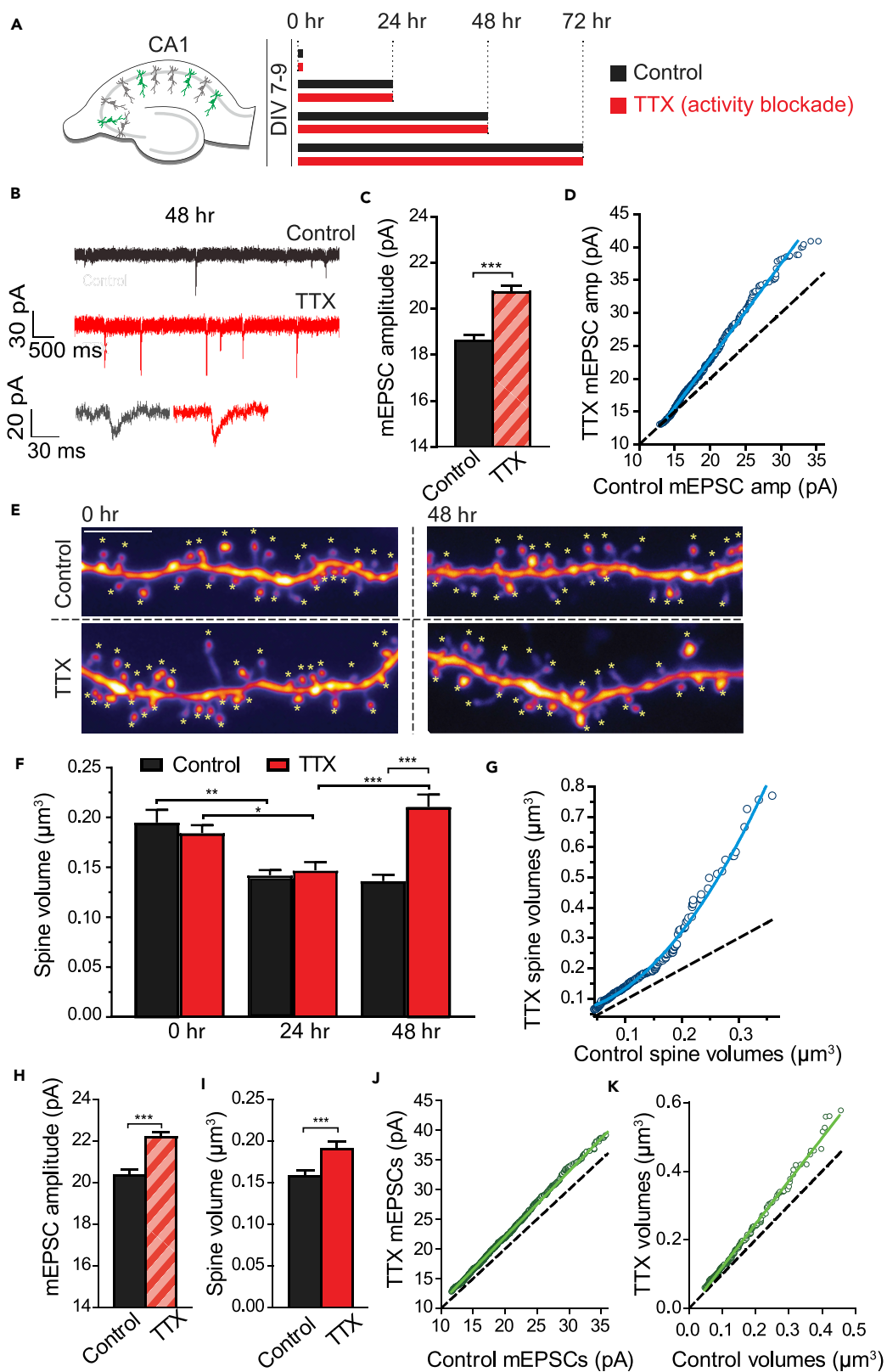


Figure 1. Spines Undergo Structural Scaling following Activity Blockade

- (A) Experimental protocol to induce HSP in hippocampal organotypic slices.
- (B) Example mEPSC recording traces from control and TTX-treated conditions at the 48 hr time point. Bottom: representative individual mEPSCs.
- (C) Quantification of mEPSC amplitudes after 48 hr of activity blockade, represented as mean \pm SEM. *** $p = 1.553 \times 10^{-8}$, Mann-Whitney. For all data presented, total number of spines or mEPSCs are represented by the first number (n) and followed by the number of independent neurons (N, in parentheses) from which they were collected. Number of mEPSCs (n) from independent neurons (N): control = 552 (8), TTX = 742 (8).
- (D) Ranked control mEPSC amplitudes plotted against TTX condition at 48 hr. Best fit line to the data: TTX = control $\times 1.45 - 6.06$.
- (E) Representative images of dendrites at either 0 or 48 hr after TTX treatment or in control media. Asterisks indicate all the spines that were analyzed. Scale bar, 5 μ m.
- (F) Quantification of spine volumes for the indicated conditions, represented as mean \pm SEM. ** $p_{0 \text{ control} - 24 \text{ control}} = 0.003$; * $p_{0 \text{ TTX-24 TTX}} = 0.03$; *** $p_{24 \text{ TTX } 48} < 0.0001$; *** $p_{48 \text{ control-48 TTX}} = 1.9e-10$. All statistics: two-way ANOVA, post-hoc Bonferroni. Number of spines (n) from independent neurons (N) for the 0, 24, and 48 hr time points: control = 103(6), 245(8), 285 (7). TTX = 172 (7), 232 (5), 208 (6).
- (G) Ranked control spine volumes plotted against TTX condition at 48 hr. Best fit line to the data: TTX = control $^2 \times 5.44 + \text{control} \times 0.25 + 0.55$.
- (H) Quantification of mEPSC amplitudes after 72 hr in TTX, represented as mean \pm SEM. *** $p = 1.883 \times 10^{-15}$, Mann-Whitney. Number of mEPSCs (n) from independent neurons (N): control = 1,164 (10), TTX = 1,302 (12).
- (I) Quantification of spine volume after 72 hr in TTX, represented as mean \pm SEM. *** $p = 0.0008$, Mann-Whitney. Number of spines (n) from independent neurons (N): control = 258 (6), TTX = 214 (6).
- (J) Ranked control 72-hr mEPSC amplitudes plotted against TTX mEPSC amplitudes. Best fit line to the data: TTX = control $\times 1.10 - 0.01$.
- (K) Ranked control 72-hr spine volumes plotted against TTX 72-hr spine volumes. Best fit line to the data: TTX = control $\times 1.26 - 0.004$.

See also Figures S1 and S2.

long-term potentiation (LTP), an increased growth rate after stimulation, and a reduced plasticity threshold. We find that HSP enhances the magnitude of synaptic potentiation through the preferential modulation of small spines and by promoting structural plasticity at clustered inputs following Hebbian activity at single synapses. Together, these changes provide a mechanism by which homeostatic plasticity can modulate synaptic efficacy and enhance future learning without compromising previously stored information.

RESULTS

Structural Correlates of Homeostatic Plasticity in Hippocampal Neurons

Hebbian plasticity at an individual input is linearly correlated with volume changes in the corresponding spine (Arellano et al., 2007; Govindarajan et al., 2011; Harvey and Svoboda, 2007; Matsuzaki et al., 2004), and thus changes in the volume of a spine can be used as a reliable proxy for functional changes at the corresponding synapse. Since HSP is known to change the functional properties of the spine, we reasoned that homeostatic modifications of efficacy should be accompanied by structural plasticity of inputs. Supporting this idea, a partial blockade of activity in the visual cortex leads to the growth of distal spines *in vivo* (Keck et al., 2013). Thus, applying a chronic activity blockade *ex vivo* in the hippocampus would allow us to model the structural consequences of homeostatic plasticity and to test how such changes affect further plasticity at single spines. We therefore induced HSP using tetrodotoxin (TTX) inhibition of sodium channels, for 0, 24, 48, or 72 hr (Figure 1A, see Transparent Methods), as this has been shown to induce scaling of synaptic strengths in a variety of systems (Karmarkar and Buonomano, 2006; Turrigiano et al., 1998). We chose to conduct our experiments in mouse hippocampal organotypic slice cultures, which maintain a physiologically relevant tissue architecture and in which the relationship between synaptic structure and function can be probed at the level of single spines. To verify that functional synaptic scaling occurred, we recorded spontaneous miniature excitatory postsynaptic currents (mEPSCs) from both TTX-treated and control CA1 hippocampal pyramidal neurons at 48 hr after the beginning of the HSP induction period (Figures 1B–1D). All recordings were performed in the presence of acute TTX to block action potentials. As expected, we found a significant increase in mEPSC amplitude following 48 hr of activity blockade (Figures 1B and 1C; control = 18.6 ± 0.25 pA, TTX = 20.72 ± 0.28 pA, $p = 1.55 \times 10^{-8}$, Mann-Whitney). The distribution of the TTX mEPSCs scaled linearly to overlay with the control distribution (Figure 1D), in accordance with the synaptic scaling theory. We next investigated whether homeostatic plasticity leads to structural modification of synapses by live, 2-photon imaging of GFP-labeled CA1 dendrites (Figure 1E). The volumes of all visible spines within the image were measured using SpineS, a custom in-house-developed MATLAB toolbox (Erdil et al., 2012; Ghani et al., 2017). We found that spines chronically treated with TTX were significantly bigger than those from control cells beginning at 48 hr (Figures 1E and 1F; control = $0.136 \pm 0.0062 \mu\text{m}^3$, TTX = $0.211 \pm 0.0123 \mu\text{m}^3$, $p = 1.9e-10$). As both control and TTX-treated spines initially reduced in volume (Figure 1F, 24 hr), it is unlikely that the spine enlargement we observe reflects an activity-induced blockade of spine shrinkage by TTX (Figure 1F; mean \pm SEM: control_{0h} = 0.195 ± 0.0125 , control_{24h} = 0.142 ± 0.005 , $p = 0.003$ [two-way ANOVA]; TTX_{0h} = 0.184 ± 0.008 , TTX_{24h} = 0.147 ± 0.008 , $p =$

0.03 [two-way ANOVA]). However, by 48 hr TTX spines were significantly bigger than the 24-hr TTX spines, and than the 48-hr control spines (Figures 1E and 1F; control = $0.136 \pm 0.0062 \mu\text{m}^3$, TTX = $0.211 \pm 0.0123 \mu\text{m}^3$, $p = 1.9e-10$; Figure S2A). Surprisingly, as opposed to the linear functional scaling of mEPSCs seen in response to HSP, we found that structural scaling of spine volumes at 48 hr are best fit to controls with a second-order equation (Figure 1G). This superlinear scaling resulted from a preponderance of large spines after TTX treatment, for which correspondingly large mEPSCs were not observed.

After 72 hr of activity blockade, synapses maintained the enhancement of mEPSC size (Figure 1H; mean \pm SEM: control 72 hr = $20.35 \pm 0.27 \text{ pA}$, TTX 72 hr = $22.18 \pm 0.239 \text{ pA}$, $p = 1.88 \times 10^{-15}$, Mann-Whitney) and spine volume increases (Figure 1I; mean \pm SEM: control = $0.16 \pm 0.0073 \mu\text{m}^3$, TTX = $0.19 \pm 0.0093 \mu\text{m}^3$, $p = 0.0008$ Mann-Whitney). However, at this time, scaling was instantiated in a linear fashion at both the level of mEPSC amplitude and spine volumes (Figures 1J and 1K). This suggests that the expression of functional and structural scaling evolves dynamically over time in response to prolonged activity blockade. We wanted to determine whether the prolonged activity blockade affected the total number of spines, and therefore we calculated spine density over days (Figure S1A). Spine density did not differ significantly over time between the control and TTX populations ($p = 0.568$, two-way ANOVA), indicating that activity blockade did not lead to an alteration in the total number of spines.

Reversibility of Homeostatic Plasticity-Mediated Structural Changes

Synaptic strength modifications that occur in response to activity blockade are reversible upon re-exposure of a circuit to activity (Desai et al., 2002; Wallace and Bear, 2004). We tested whether the structural changes that resulted following activity blockade were also reversible when activity is restored. After 48 hr of homeostatic plasticity induction, by which time significant structural and functional scaling have occurred (Figure 1), we removed TTX allowing slices to resume activity and measured spontaneous firing using whole-cell patch-clamp recordings (Figures 2A and 2B). Activity blockade for 48 hr led to higher firing rates compared with untreated cells (Figure 2C; control [median] = 1.33, IQ range = 0.11:18.83 spikes/min; TTX [median] = 13.33, IQ range = 11.5:21.06 spikes/min; $p = 0.03$, Kruskal-Wallis post-hoc Dunn). To exclude the possibility that the higher firing rates we observed were due to a rebound after the acute withdrawal of TTX from the system, a set of control neurons were briefly incubated in TTX (2–4 hr, named “acute TTX condition”). This manipulation did not significantly alter firing rates, which were similar to untreated controls (Figure 2C; acute TTX: median = 4.44, IQ range = 2.0:29.33 spikes/min versus control no TTX: median = 1.33, IQ range = 0.11:18.83 spikes/min, $p > 0.9$ Kruskal-Wallis post-hoc Dunn). Thus the firing rate changes we observed were the result of HSP and did not arise from the acute withdrawal of TTX. We then investigated whether the circuit would return to its original level of activity once neurons were released from blockade. Indeed, after having removed TTX for 48 hr, firing rates were indistinguishable from controls (Figure 2C; control [median] = 1.33, IQ range = 0.11:15.56. TTX reversal [median] = 1.67, IQ range = 0.194:11.76. $p > 0.05$, Kruskal-Wallis post-hoc Dunn). We then examined whether structural modifications accompanied these firing rate changes, and observed a similar reversal in spine volumes (Figures 2D and 2E). TTX-treated spines significantly reduced in size 48 hr after TTX removal (Figure 2E; mean volume \pm SEM: TTX 48 hr = $0.21 \pm 0.0063 \mu\text{m}^3$; TTX 48 hr reversal = $0.16 \pm 0.0064 \mu\text{m}^3$, $p = 4.1852 \times 10^{-7}$). These findings support the idea that functional plasticity is matched by structural plasticity and that spine sizes reversibly and accurately reflect the activity landscape.

Enhanced Hebbian Potentiation of Small Spines after Homeostatic Plasticity

Functional plasticity can be enhanced upon homeostatic modulation in hippocampal slices (Arendt et al., 2013; Félix-Oliveira et al., 2014), but occlusion of LTP may also occur (Soares et al., 2017). Given our finding that robust growth of spines occurs during homeostatic plasticity, we wanted to determine whether individual inputs were able to undergo further activity-dependent structural plasticity. We therefore induced HSP in hippocampal slices for 48 hr and followed this with synaptic potentiation at visually identified dendritic spines through 2-photon-mediated glutamate uncaging (Figures 3A and 3B; see *Transparent Methods*). This paradigm elicits potentiation and growth of only the stimulated input, but not the nearby neighboring spines (Govindarajan et al., 2011; Harvey and Svoboda, 2007). We followed the growth of spines relative to their average baseline volumes, in both the TTX and control conditions (Figures 3C and 3D), and compared with the unstimulated neighboring spines. During the initial 45 min post-stimulation, both TTX-treated and control spines grew to a similar extent, indicating that homeostatic structural scaling does not occlude activity-dependent structural plasticity (mean \pm SEM; control stimulated 45' = 1.45 ± 0.10 ; control neighbors 45' = 1.08 ± 0.04 ; TTX stimulated 45' = 1.59 ± 0.14 ; TTX

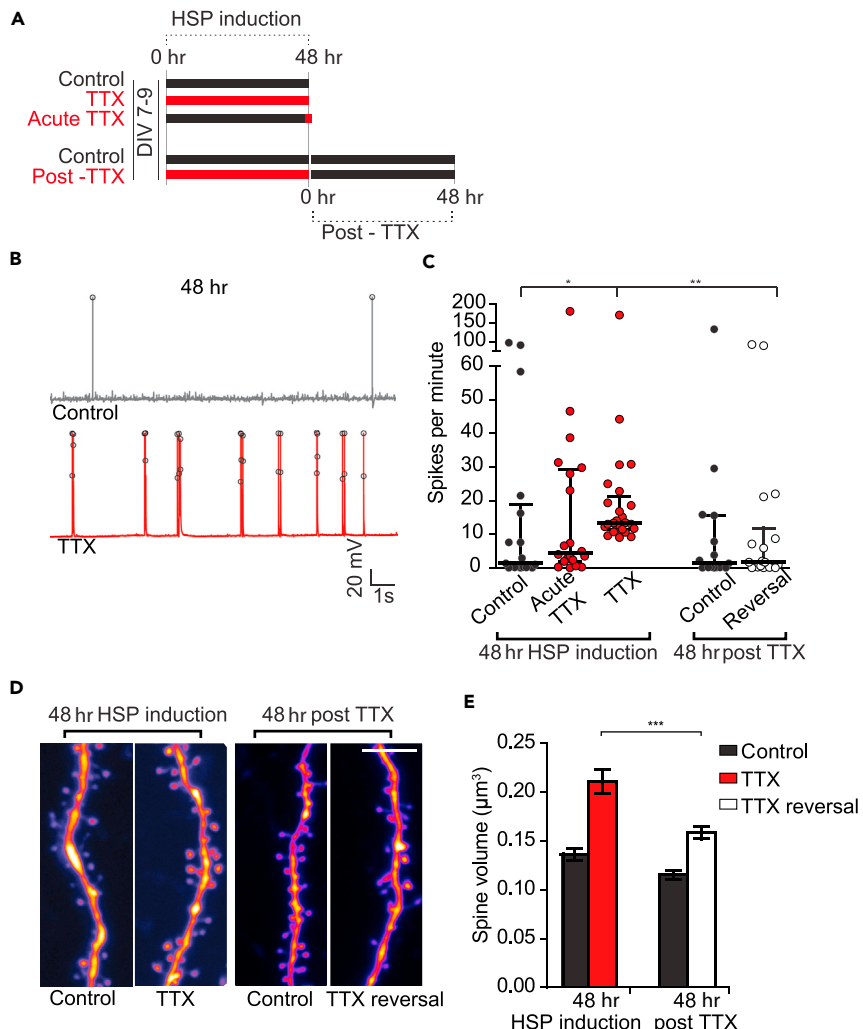


Figure 2. Structural and Functional Changes after HSP Are Reversible

(A) Experimental timeline for reversal experiments.

(B) Example traces showing cell firing following 48 hr of activity block. Spikes are demarcated with black circles.

(C) Quantification of spikes per minute throughout experiment, represented as median + IQ range. * $p_{48 \text{ control}-48 \text{ TTX}} = 0.03$, Kruskal-Wallis post-hoc Dunn; ** $p_{48 \text{ TTX}-48 \text{ post TTX}} = 0.010$, Kruskal-Wallis post-hoc Dunn. Number of neurons: 48 hr TTX condition: 48 hr control = 17, 48 hr acute TTX = 20, 48 hr TTX = 26; 48 hr “post-TTX” control = 15, 48 hr post-TTX reversal = 18.

(D) Representative images from dendrites after 48 hr of HSP induction and at 48 hr post TTX. Scale bar, 5 μm .

(E) Quantification of spine sizes throughout the experiment, represented as mean \pm SEM. All p values calculated using Kruskal-Wallis test, post-hoc Dunn's. *** $p_{48 \text{ TTX}-48 \text{ post TTX}} = 4.1852 \times 10^{-7}$. Number of spines (n = first number) of neurons (N = in parentheses): 48 hr control = 285 (7), 48 hr TTX = 208 (6), 48 hr “post-TTX” control = 514 (14), 48 hr post-TTX = 430 (15).

neighbors $45' = 1.14 \pm 0.04$; $p > 0.99$ (Figure 3D). However, after 120 min, only the stimulated inputs in the TTX-treated neurons remain significantly larger than their neighbors (Figure 3D; mean \pm SEM: TTX stimulated $120' = 1.53 \pm 0.13$; TTX neighbors $120' = 1.16 \pm 0.04$), as control spines begin to return to their initial volume (Figure 3D; control stimulated $120' = 1.30 \pm 0.01$; control neighbors $120' = 1.14 \pm 0.04$). Although the TTX and control spines are not significantly different at $120'$ ($p = 0.1345$, Mann-Whitney), they begin to diverge, as seen relative to their respective neighbors. Thus, at scaled synapses, activity that would otherwise lead to short-lived structural plasticity now elicits long-lasting structural plasticity.

Structural plasticity at individual inputs varies with activity and spine size. Weak stimulations preferentially affect small spines (Matsuzaki et al., 2004), whereas strong stimuli can elicit structural plasticity across a

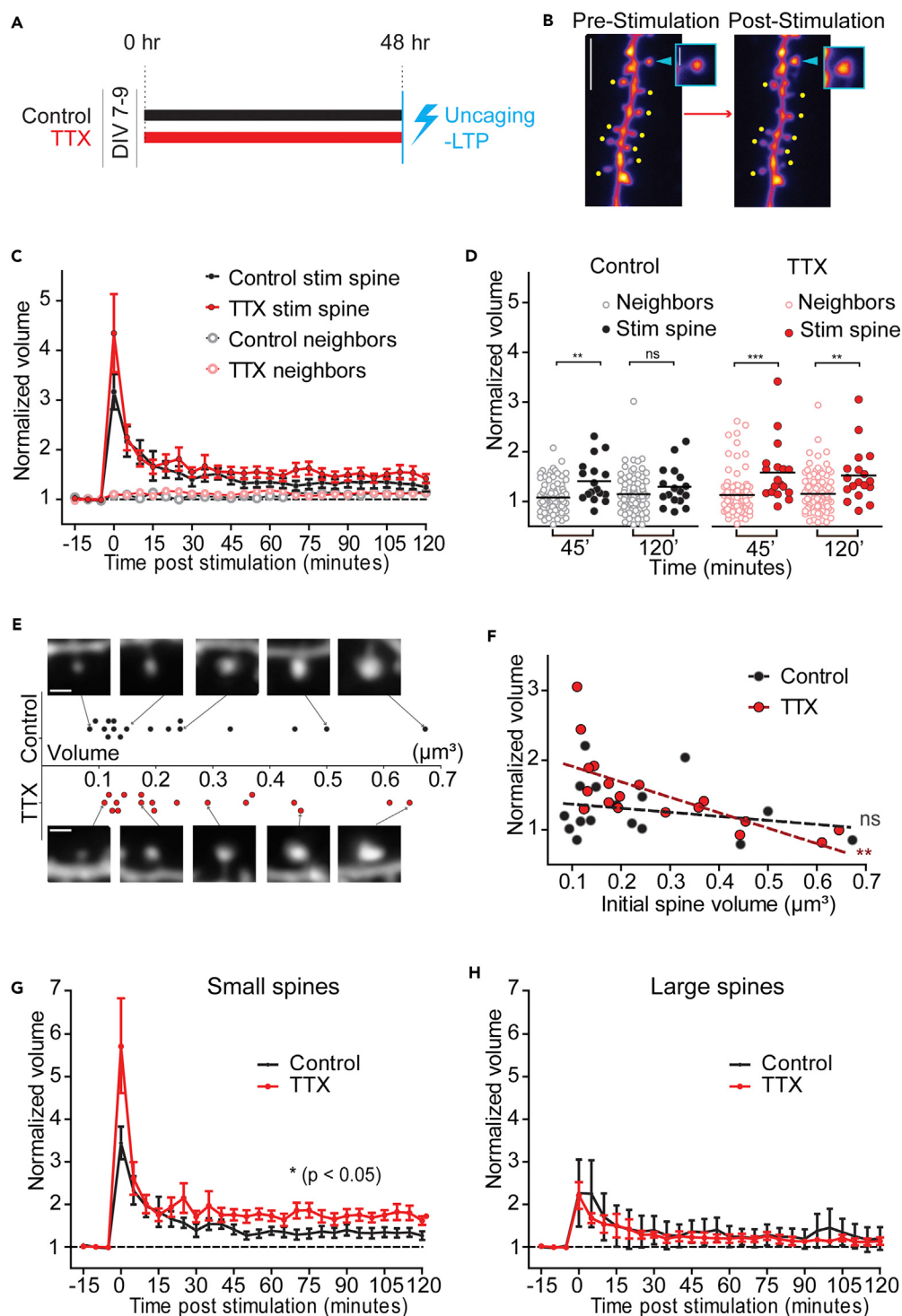


Figure 3. Potentiation of Single Inputs Is Enhanced at Smaller Spines following HSP

(A) Timeline for uncaging experiments.

(B) Representative images of structural plasticity following single spine glutamate uncaging. Arrowheads and dots indicate stimulated and neighboring non-stimulated spines, respectively. Scale bar, 5 μm (main image), 1 μm (inset). (C) Normalized volume of stimulated and neighboring spines for control and TTX-treated conditions over 2 hr of LTP induction, represented as mean + SEM. Volumes were calculated from Z-stacks taken in 5-min bins from time point 0 (thus the stack represented as 0 was collected between 0 and 5 min, for example). For all data, the total number of spines are

Figure 3. Continued

represented by the first number (n), and followed by the number of independent neurons (N = in parentheses) from which they were collected. Control stimulated = 17 (17), TTX stimulated = 18 (18), control neighbors = 85 (17), TTX neighbors = 102 (18).

(D) All analyzed stimulated and neighboring spine volumes at time points 45 min and 120 min post-stimulation, with the mean marked. Significance was calculated using one-way ANOVA post-hoc Bonferroni. Control condition:

$**P_{\text{stimulated}45-\text{neighbors}45} = 8.4246 \times 10^{-4}$; $P_{\text{stimulated}120-\text{neighbors}120} = 0.6881$. TTX condition: $***P_{\text{stimulated}45-\text{neighbors}45} = 2.9383 \times 10^{-4}$. $**P_{\text{stimulated}120-\text{neighbors}120} = 0.0046$ [n same as in (C)].

(E) Distribution of all initial volumes of stimulated spines, with example spine images. The cutoff for defining “large” spines was the median volume off all spines multiplied by 1.5. Scale bar, 1 μm .

(F) Initial absolute spine size versus normalized spine volume at 120 min. TTX spines linear regression: $r^2 = 0.48$, $**p = 0.002$. Control linear regression: $r^2 = 0.06$, $p = 0.346$.

(G) Time course of the structural LTP experiment plotting only the small spines, represented as mean +SEM. $*p = 0.0458$, two-way repeated measures ANOVA. Number of spines (n) from neurons (N, in parentheses): control = 13 (13), TTX = 11 (11).

(H) Time course of structural LTP plotting only large spines, represented as mean +SEM. $p = 0.699$, two-way repeated measures ANOVA. Number of spines (n) from neurons (N, in parentheses): control = 4 (4), TTX = 17 (17).

See also Figure S2.

variety of spine sizes (Govindarajan et al., 2011; Oh et al., 2013; Ramiro-Cortés and Israely, 2013). Our stimulated spines spanned a range of sizes, allowing us to test whether size interacted with prior expression of HSP when expressing synaptic potentiation and further spine growth (Figure 3E). We examined the amount of structural plasticity expressed by spines of different initial sizes after activity blockade. We found a negative correlation between a spine’s initial average value and its normalized final volume when the spine population had first undergone homeostatic plasticity, but not in the control population, indicating that spine volume is an important modulator of the potential for plasticity after HSP (Figures 3E and 3F; $r^2 = 0.48$ for TTX, $p < 0.01$, $r^2 = 0.06$ for control, $p > 0.3$). To further examine how HSP modulates the size dependence of structural plasticity, we classified spines as “large” if their initial volume was more than 150% of the median initial volume of all spines, and the remainder were placed in the “small” category. This latter group did not fall below the 25th percentile of the entire distribution, as can be seen in the plot of all the experimental spines’ initial volumes relative to the population from which they were drawn (Figures S2A and S2B). Among the small spines, we observed a significant increase in the magnitude of LTP in the TTX condition compared with the controls (Figure 3G; $p = 0.046$, 2-way repeated measures ANOVA). On the other hand, large spines expressed a short-lasting growth that quickly decayed to baseline and was not dependent on whether they had been subjected to activity blockade (Figure 3H; $p = 0.70$, 2-way repeated measures ANOVA). Therefore, small spines preferentially underwent long-lasting structural plasticity after HSP. We further observed that small spines, which had undergone HSP, tended to show a greater degree of initial growth in response to the induction of plasticity (Figure 3G, time point 0). To quantify the dynamic growth of these spines, we analyzed high-speed images of the spine head taken throughout the stimulation period (approximately 20 Hz) and did not observe a significant difference in the growth curves between the control and TTX-treated spines (Figures 4A and 4B). When we examined the rate of growth that each spine expressed in the first minute after the stimulation, however, we found that TTX-treated small spines grew more than control small spines (Figure 4C; $p = 0.018$, one-way ANOVA with post-hoc Tukey’s), whereas large spines showed no difference between the two conditions. Therefore, glutamate stimulation leads to a sustained growth of homeostatically modified small spines, which may reflect prolonged signaling at these synapses. Together, these data indicate that HSP facilitates Hebbian plasticity and that this is accomplished at the individual spine level through preferential structural plasticity of small inputs.

Homeostatic Plasticity Facilitates the Induction of Hebbian Structural Plasticity

Having observed that small spines showed enhanced responses to stimulation after homeostatic plasticity, as reflected by a higher rate of growth and longer lasting structural plasticity (Figures 3G and 4C), we reasoned that these inputs may respond more robustly to a weaker stimulation. This is also supported by previous findings that loss of activity at individual inputs lowers their threshold for subsequent plasticity (Lee et al., 2010). To test this possibility, we applied a subthreshold stimulation that utilizes a shorter laser pulse of 1 ms (instead of 4 ms) during the glutamate uncaging protocol, since this does not induce structural plasticity at spines (Govindarajan et al., 2011; Harvey and Svoboda, 2007). Indeed, control spines that underwent this subthreshold stimulation showed only a transient post-stimulus growth that lasted 5 min, resulting in no long-term plasticity (Figure 4D; control spines, 1 ms stimulated versus neighbors: $p > 0.05$, 2-way repeated measures ANOVA, post-hoc Bonferroni). These results were significantly different

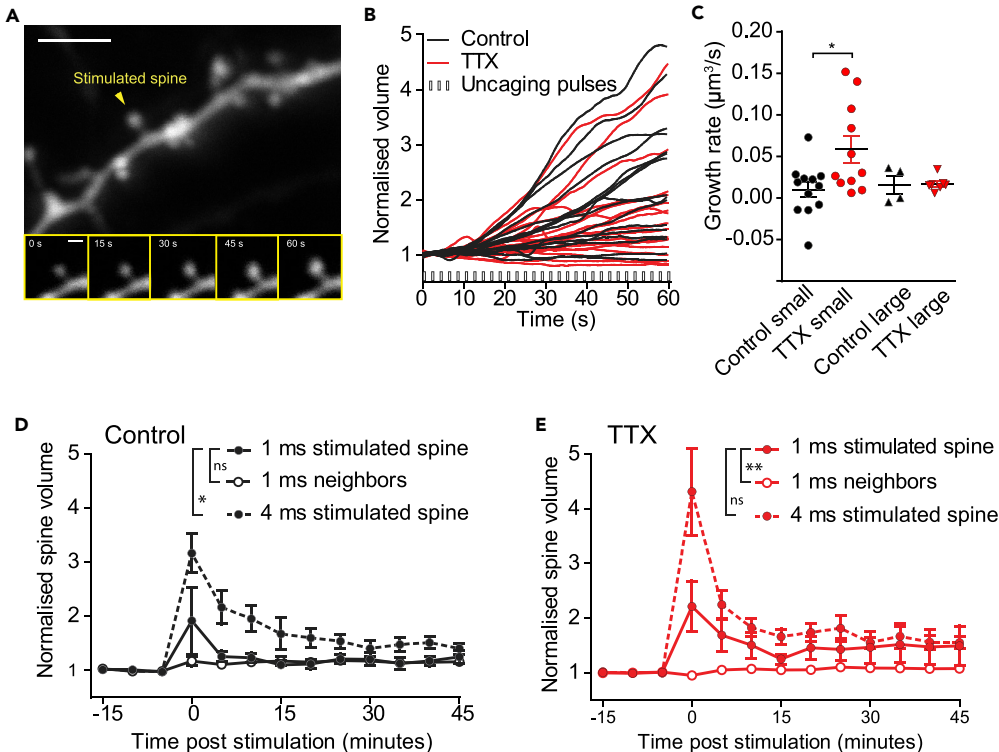


Figure 4. HSP Increases the Efficacy and Reduces the Threshold for Induction of LTP at Individual Spines

(A) Representative image of a single spine during the course of uncaging. Scale bar, 5 μm (main image), 1 μm (inset). (B) Individual traces of spine growth during glutamate uncaging stimulation. Control spine growth versus TTX spine growth: $p = 0.198$, two-way repeated measures ANOVA. Number of spines (n): control = 16, TTX = 18.

(C) Growth rates of stimulated spines for 1 min after the end of stimulation, represented as mean + SEM. * $p_{\text{small control-small TTX}} = 0.018$, one-way ANOVA with post-hoc Tukey's. $p_{\text{large control-large TTX}} < 0.99$, one-way ANOVA with post-hoc Tukey's. Number of spines (n): control small = 13, TTX small = 11, control large = 4, TTX large = 7.

(D) Quantification of normalized spine volume with different stimulation pulse durations in the control condition, represented as mean + SEM. $p_{\text{1ms stimulated-1ms neighbors}} = 0.292$, two-way repeated measures ANOVA post-hoc Bonferroni. Number of spines (n) from neurons from which they were collected (N, in parentheses): stimulated 1 ms = 11 (11), neighbors 1 ms = 52 (11), stimulated 4 ms = 17 (17). * $p_{\text{1ms stimulated-4ms stimulated}} = 0.039$; two-way rm ANOVA. Note 4 ms data are the same as shown in Figure 3.

(E) Quantification of normalized spine volume with different stimulation pulse durations in the TTX condition, represented as mean + SEM. ** $p_{\text{1ms stimulated-1ms neighbors}} = 0.007$, two-way rm ANOVA. $p_{\text{1ms stimulated-4ms stimulated}} = 0.27$, two-way rm ANOVA. Number of spines (n) from neurons (N): stimulated 1 ms = 11 (11), neighbors 1 ms = 52 (11), stimulated 4 ms = 18 (18). Note 4 ms data are the same as in Figure 3.

from what we had observed in response to the 4-ms stimulation (Figure 4D; 1 ms stimulated versus 4 ms stimulated; $p = 0.04$, 2-way repeated measures ANOVA; compared with data from Figure 3C). In contrast to this, HSP-modified spines grew significantly in response to the subthreshold stimulation and remained larger than their neighbors (Figure 4E; TTX spines, 1 ms stimulated versus neighbors, $p = 0.01$, 2-way repeated measures ANOVA, post-hoc Bonferroni). Following TTX treatment, both weak and strong stimulations elicited similar levels of long-lasting growth of spines (Figure 4E; 1 ms stimulated versus 4 ms stimulated: $p = 0.27$, 2-way repeated measures ANOVA). Thus, homeostatic plasticity facilitates structural plasticity by lowering the threshold for stimulation, without affecting the magnitude of plasticity. In this way, HSP acts locally, in conjunction with activity, to increase the likelihood that an individual synapse will participate in the encoding of information.

Homeostatic Plasticity Influences Structural Plasticity of Neighboring Spines

In addition to modifying synaptic inputs through scaling, homeostatic plasticity can also influence cellular firing rates by modulating the intrinsic excitability of neuronal membranes (Desai et al., 1999). We reasoned that such alterations could facilitate the expression of structural plasticity not only at stimulated spines but

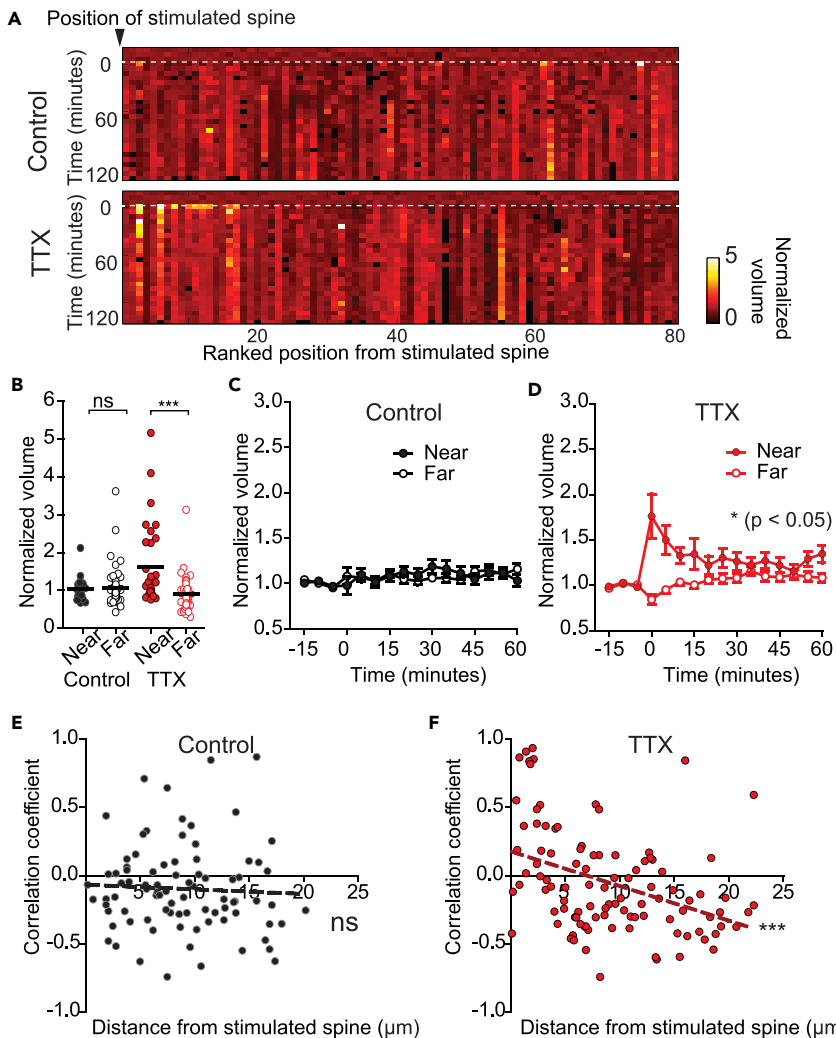


Figure 5. Stimulation of Single Inputs Leads to Plasticity of Clustered Neighbors after HSP

(A) Heat maps of growth dynamics of neighboring spines over time. Neighbors from all experiments were pooled and ranked in order of distance from the stimulated spine. Index 1 is the spine nearest to its stimulated spine, and 80 is the furthest away. Heatmap = normalized spine volume. Number of spines (n) from neurons from which they were collected (N, in parentheses): control = 80 (17), TTX = 80 (18).

(B) Normalized spine volumes for the first 10 min following stimulation for the different neighboring conditions, with the mean marked. *** $p_{\text{TTX near-TTX far}} = 3.66 \times 10^{-6}$; $p_{\text{Control near-Control far}} > 0.99$, Kruskal-Wallis. Number of spines (n) from neurons from which they were collected (N, in parentheses): control near = 22 (17), control far = 63 (17), TTX near = 32 (18), TTX far = 70 (18).

(C) Normalized volumes of near and far neighboring spines in the control condition, represented as mean + SEM. $p = 0.987$, two-way rm ANOVA. Number of spines same as above.

(D) Normalized volumes of neighboring spines in the TTX condition, represented as mean + SEM. * $p = 0.0124$, two-way repeated measures ANOVA. Number of spines same as above.

(E and F) Correlation coefficients of volume change of stimulated spines versus volume change of neighboring spine, plotted against the distance between the neighboring spine and the stimulated spine. (E) Linear regression control: $r^2 = 0.003$, $p = 0.641$. (F) Linear regression TTX: $r^2 = 0.156$, *** $p = 3.91 \times 10^{-5}$.

See also Figure S3.

also at nearby inputs within the dendritic branch. To test this idea, we examined whether homeostatic plasticity altered neighboring spine volume dynamics following the potentiation of single inputs. We ranked neighboring spines according to their distance from the stimulated spine (with 1 representing the closest neighbor to a stimulated spine) and plotted their growth dynamics for 2 hr following the stimulation (Figure 5A). We found that spines located in close proximity to the stimulated spine increased in volume only in

neurons that had first undergone homeostatic plasticity (compare the first 20 spines, from 0 to 60 min after stimulation, [Figure 5A](#)). We classified the unstimulated neighbors as “near” or “far”—located either within or beyond 5 μm of the stimulated spine, respectively—and quantified spine volume changes over time ([Figures 5B–5D](#)). As expected, none of the neighbors of stimulated spines changed significantly from their original size in untreated neurons ([Figures 5B and 5C](#)). However, after HSP, neighbors that were within 5 μm of the target spine exhibited significant growth in the 5 min following the stimulation ([Figure 5B](#)) and remained significantly larger than more distant spines ([Figures 5B and 5D](#); $p = 0.001$, two-way repeated measures ANOVA). Interestingly, farther neighbors (located up to 20 μm away from the site of stimulation) tended to decrease in size for several minutes following activity, although this was not significantly different from baseline ([Figure 5D](#)). Given that neighboring spines grew, whereas distal spines tended to shrink, we did not find a significant difference in the mean spine volumes at the level of the dendritic branch between control and TTX-treated neighbors ([Figure S3](#); $p = 0.573$, two-way ANOVA). We next investigated whether there was a correlation between the structural dynamics of each stimulated spine and its neighbors. We calculated correlation coefficients between the volume change of the stimulated spine and those of its neighbors across the time course of the experiment. Fluctuations in the volumes of neighboring spines in control conditions were independent of the stimulated input ([Figure 5E](#); $r^2 = 0.00263$, $p = 0.61$), whereas spine volumes in TTX-treated neurons changed in accordance with the stimulated spine ([Figure 5F](#); $r^2 = 0.156$, $p < 0.001$). Specifically, near-TTX neighbors had a positive correlation with the stimulated input, reflecting growth, which eventually became a negative correlation at further distances from the stimulated spine. These findings indicate that HSP reduces the input specificity of activity in a distance-dependent manner that is simultaneously cooperative with near and competitive with far inputs. This allows for homeostatic modulation to effect structural plasticity within a dendritic region through activity at a single spine, which favors clustered plasticity of synaptic inputs.

DISCUSSION

Synaptic networks must balance the need to enhance efficacy during learning without saturating their capacity for further changes. Homeostatic plasticity can achieve this regulatory role by effecting a gain modulation on neurons to maintain synaptic activity within an optimal target range. The consequences of implementing HSP for the network, and specifically, the effect of its interaction with Hebbian plasticity on the subsequent encoding of information at the level of single inputs, is unclear. Due to the linear relationship between synaptic structure and function, we used live 2-photon imaging and glutamate uncaging to probe the physical consequences of inducing homeostatic plasticity on a neuron, and to determine how this affects the ability of single synapses to undergo further changes in efficacy. We show that HSP, induced by 48 hr of activity blockade, leads to the reversible growth of dendritic spines. We demonstrate that this form of modulation facilitates subsequent structural plasticity at single synapses and that this effect preferentially occurs at smaller inputs. After HSP, activity elicits a faster growth rate at these spines and converts an otherwise sub-threshold stimulation into one that is now capable of eliciting structural plasticity. Interestingly, we find that the induction of Hebbian plasticity on a background of homeostatic plasticity leads to compromised input specificity, as neighboring spines grow when they are located in close proximity to a stimulated synapse. Taken together, our results show that homeostatic plasticity can modulate a neuron’s response to activity by facilitating the sensitivity of smaller inputs and inducing structural plasticity at neighboring synapses.

The structural scaling that we observe after 48 hr of activity blockade results in a non-linear upscaling of spines and an increased number of large spines ([Figure 1G](#)). By 72 hr, this structural scaling becomes linear ([Figure 1K](#)), suggesting that the initial changes may represent a physical overshooting of the target size. This has also been observed on short timescales following glutamate stimulation of single spines, where an initial large volume change is followed by stabilization of the spine at a more modest size ([Matsuzaki et al., 2004](#)). Of interest, an overshoot of cellular responses has been described during recovery from visual deprivation, suggesting that exaggerated responses of both structural and functional modifications may be a feature of the convergence of Hebbian and homeostatic plasticity ([Toyoizumi et al., 2014](#)). Upon the reinstatement of activity, we find that spines return to their original size as firing patterns normalize by 48 hr ([Figures 2C–2E](#)), indicating that homeostatic structural changes are plastic and reversible, similarly to homeostatic responses to alterations in activity levels.

We demonstrate that activity blockade increases spine sizes across the population, raising the question of whether further enhancement of potentiation and spine growth could be achieved across inputs of different sizes. Both enhancement and occlusion of plasticity have been reported following HSP at the

population level (Arendt et al., 2013; Félix-Oliveira et al., 2014; Soares et al., 2017), but it is unclear how individual inputs are modulated. Furthermore, although larger synapses have been shown to undergo functional homeostatic modulation (Thiagarajan et al., 2005), inputs show a size-dependent variation in their ability to undergo Hebbian structural plasticity, large spines being more stable and requiring stronger stimulation to be potentiated (Govindarajan et al., 2011; Matsuzaki et al., 2004). We probed plasticity with glutamate uncaging and found that HSP leads to structural plasticity lasting over 2 hr preferentially at small spines, whereas control spines decay to baseline after 1 hr (Figures 3G and 3H). This indicates that after HSP a long-lasting, protein-synthesis-dependent form of Hebbian plasticity was induced at these inputs, whereas a shorter, protein-synthesis-independent form was induced in controls, based on the differential longevities of structural plasticity (Govindarajan et al., 2011). Several lines of evidence point to the involvement of new protein synthesis during homeostatic plasticity. The specific production of plasticity-related proteins has recently been shown to occur following activity blockade with TTX (Schanzenbacher et al., 2018), and a mechanistically distinct form of HSP acting through retinoic acid receptors is also known to induce new protein synthesis (Aoto et al., 2008; Sutton et al., 2006). Furthermore, activation of group 1 metabotropic glutamate receptors by Homer1A leads to ERK- and mammalian target of rapamycin-dependent protein translation during homeostatic scaling (Hu et al., 2010). These studies suggest that protein synthesis is likely to be a crucial component of homeostatic responses, similar to its role in the maintenance of long-term plasticity changes (Costa-Mattioli et al., 2009).

Closer examination of the structural plasticity we induced revealed that the population of small spines express the majority of the growth, whereas large spines remain stable (Figures 3G and 3H). This result implies that while homeostatic modifications may increase the absolute number of large spines, plasticity at these inputs is saturated to an equal extent irrespective of whether they had undergone activity blockade, and their threshold for structural plasticity is not further altered by HSP. Upon stimulation, we did not observe a significant difference in the magnitude of the potentiation that spines expressed, nor in their immediate response to the stimulation itself, but rather we found that spines post-HSP express a significantly faster growth rate compared with their counterparts in the first minute after stimulation (Figures 4A–4C). This enhanced response may be due to amplified signaling cascades shared between these forms of plasticity (Fernandes and Carvalho, 2016), which could facilitate the induction of long-lasting structural plasticity. It was therefore not surprising to find that a subthreshold stimulation elicits long-lasting growth only at inputs that have undergone homeostatic plasticity (Figures 4D and 4E), without affecting the initial magnitude of the response between the HSP-modified synapses and the control populations. Changes to N-methyl-D-aspartate receptor composition that occur following activity blockade could provide a means by which to enhance the calcium permeability of synapses and thus would allow for prolonged signaling responses (Barria and Malinow, 2005; Lee et al., 2010; Paoletti et al., 2013). Taken together, these data show that the effects of homeostatic plasticity preferentially affect small spines during Hebbian regulation of synaptic strength by predisposing them to undergo long-lasting structural changes. Such modulation may result in the conversion of weaker stimuli into more salient forms and proposes a more global role for HSP in information encoding beyond the optimization of neuronal activity.

A hallmark of activity-dependent changes during Hebbian plasticity is input specificity (Barrionuevo and Brown, 1983). In contrast, homeostatic plasticity is generally expressed over a wider synaptic range, although local homeostatic changes can also occur at the dendritic level (Branco et al., 2008; Ju et al., 2004; Liu, 2004; Sutton et al., 2006). How such modulation affects Hebbian learning rules at individual inputs is unknown (Vitureira and Goda, 2013), but computational studies have postulated that homeostatic plasticity can influence previous Hebbian events at a synapse (Rabinowitch and Segev, 2008). We therefore considered the analogous possibility that HSP may function to influence subsequent Hebbian plasticity, beyond the stimulated synapse. Indeed, we find that HSP induces the spillover of Hebbian structural plasticity within the dendrite, as seen by the growth of neighboring unstimulated spines following the activation of one input (Figure 5). Thus, homeostatic plasticity drives the local expression of Hebbian plasticity and reduces input specificity. Mechanistically, the high degree of overlap between pathways leading to the expression of Hebbian and homeostatic plasticity may facilitate such interactions. Most prominently among these is the modulation of synaptic strength through changes in AMPA receptor content in the postsynaptic density, which occurs during both forms of plasticity (Huganir and Nicoll, 2013; O'Brien et al., 1998). Furthermore, a variety of proteins that regulate AMPA receptor localization and retention in the post-synaptic density (PSD) have been shown to play a role in both Hebbian and homeostatic plasticity, such as the activity-dependent protein Arc/Arg2.1, PSD-95, and other PDZ domain-containing proteins

such as PICK1 and GRIP1 (for review, see: [Fernandes and Carvalho, 2016](#); [Yee et al., 2017](#)). These may serve to regulate either the number or the subtype of AMPA receptors present at the synapse in an activity-dependent manner, and if acting at the branch level, may influence subsequent Hebbian plasticity. In addition, pathways classically associated with the expression of Hebbian plasticity, such as CamKII activation of SynGAP and thus Ras ([Komiyama et al., 2002](#)), have recently been linked to homeostatic plasticity via SynGAP-mediated suppression of protein translation ([Wang et al., 2013](#)). By directly impinging on ERK-Ras activity, this may represent one mechanism by which homeostatic plasticity can influence Hebbian plasticity at neighboring inputs. It remains to be determined how these processes are regulated to achieve both neuronal stability and information storage.

Although cooperative interactions have been shown to occur between inputs when multiple synapses are stimulated ([Govindarajan et al., 2011](#); [Harvey and Svoboda, 2007](#)), in the absence of such co-activation, structural changes at neighbors have thus far served to counterbalance the direction of plasticity ([Oh et al., 2015](#)). Our observations that HSP promotes activity-driven growth of a group of synapses within a 5-μm area is in alignment with the observed distance and time over which plasticity-related proteins, such as Ras, can spread between co-active synapses ([Harvey et al., 2008](#); [Harvey and Svoboda, 2007](#)). Following activity at a single spine, the movement of Ras in particular has been shown to spread locally in the dendrite and to effect a reduction in the threshold of plasticity at neighbors. As signaling by brain-derived neurotrophic factor, which leads to Ras-ERK activation, plays a role in both Hebbian and homeostatic plasticity ([Korte et al., 1998](#); [Rutherford et al., 1998](#); [Wang et al., 2013](#)), it is possible that Ras activity represents a mechanistic point of convergence that allows for the spread of LTP following HSP. Some of the signaling events related to Ras and Rho activation can now begin to be elucidated by taking advantage of new fluorescence resonance energy transfer-based sensors that allow for the visualization of ERK and PKA kinases ([Tang and Yasuda, 2017](#)), which can travel for over 10-μm along the dendrite, matching well with the parameters over which we observe metaplasticity between spines. It will be interesting to assess whether the spatial and temporal spread of Ras is altered following activity blockade.

The interaction between homeostatic and Hebbian plasticity may coordinately delimit a region of clustered plasticity, which has been proposed to increase the memory capacity of a neural circuit ([Chklovskii et al., 2004](#); [Govindarajan et al., 2011, 2006](#); [Ramiro-Cortés et al., 2014](#)). Although clustered activity and its structural correlates have begun to emerge ([Fu et al., 2012](#); [Govindarajan et al., 2011](#); [Kleindienst et al., 2011](#); [Makino and Malinow, 2011](#); [Yadav et al., 2012](#)), the mechanisms that drive the physical organization of inputs are still unknown. HSP may provide a basis for such organization by reducing the threshold for cooperativity between inputs, allowing primed synapses located within several microns of an active spine to be more easily potentiated. This may serve as a first step in the physical arrangement of synapses into clusters. The broader consequence of this could be the binding together of information of varying saliences, within a delimited region, into the same engram.

Our finding that synaptic threshold modulation after HSP is implemented at small, rather than at large spines, and in a reversible manner, suggests that synaptic scaling mechanisms are separable from plasticity mechanisms. However, by promoting long-lasting plasticity at select spines, and potentiating unstimulated neighboring spines within a delimited dendritic region, homeostatic plasticity may interact with and reduce the input-specific nature of Hebbian plasticity, enhance the clustering of synaptic inputs, and shape the long-term organization of neural circuits. In this way, despite the global nature of homeostatic plasticity, inputs may be locally modulated in an activity-dependent manner.

Limitations of the Study

The linear correlation between the structural properties of a spine (i.e., volume) and the functional ones (i.e., conductance) have been repeatedly demonstrated ([Arellano et al., 2007](#); [Govindarajan et al., 2011](#); [Harvey and Svoboda, 2007](#); [Matsuzaki et al., 2004](#)). This allows for changes in spine volume to be used as a proxy for quantifying changes in functional plasticity. Indeed, we have previously shown that when spine current amplitude is measured hours after the induction of structural plasticity, the linear scaling of size with current amplitude is maintained ([Govindarajan et al., 2011](#)). Nevertheless, we cannot formally exclude the possibility that some of the changes induced upon homeostatic plasticity may alter this structure-function relationship. Although it is not currently possible to follow functional changes at individual inputs over many days, it would be interesting to observe in real time the dynamic fluctuations in a spine's

structural and functional properties in response to changes in activity. In addition, since the complete blockade of all activity *in vivo* cannot be achieved, we could not test the interplay between homeostatic and Hebbian plasticity at single spines in this context, something that would be of interest to evaluate in the future.

METHODS

All methods can be found in the accompanying [Transparent Methods supplemental file](#).

SUPPLEMENTAL INFORMATION

Supplemental Information includes Transparent Methods and three figures and can be found with this article online at <https://doi.org/10.1016/j.isci.2018.09.015>.

ACKNOWLEDGMENTS

We thank Ali Ozgur Argunsah for advice and help with data analysis. We thank Gil Costa for design help with the figures and the graphical abstract. We thank Steven Kushner, Rui Costa, and members of the Israely laboratory for their support and critical reading of the manuscript. This work was supported by grants from the Fundação Bial (161/10-2010 to I.I.), Fundação para a Ciência e a Technologia (PTDC/SAU-NMC/122035/2010 to I.I.; SFRH/BD/51265/2010 to A.H.), and Consejo Nacional de Ciencia y Tecnología (254878 to Y.R.C.).

AUTHOR CONTRIBUTIONS

A.F.H., Y.R.C., and I.I. designed the experiments and built the setup. A.F.H. performed the experiments and analyzed the data. A.F.H. and I.I. wrote the manuscript.

DECLARATION OF INTERESTS

The authors declare no competing interests.

Received: May 15, 2018

Revised: August 3, 2018

Accepted: September 17, 2018

Published: October 26, 2018

REFERENCES

- Aoto, J., Nam, C.I., Poon, M.M., Ting, P., and Chen, L. (2008). Synaptic signaling by all-trans retinoic acid in homeostatic synaptic plasticity. *Neuron* 60, 308–320.
- Arellano, J.I., Benavides-piccione, R., Defelipe, J., and Yuste, R. (2007). Ultrastructure of dendritic spines: correlation between synaptic and spine morphologies. *Front. Neurosci.* 1, 131–143.
- Arendt, K.L., Sarti, F., and Chen, L. (2013). Chronic inactivation of a neural circuit enhances LTP by inducing silent synapse formation. *J. Neurosci.* 33, 2087–2096.
- Barnes, S.J., Franzoni, E., Jacobsen, R.I., Erdelyi, F., Szabo, G., Clopath, C., Keller, G.B., and Keck, T. (2017). Deprivation-induced homeostatic spine scaling *in vivo* is localized to dendritic branches that have undergone recent spine loss. *Neuron* 96, 871–882.e5.
- Barria, A., and Malinow, R. (2005). NMDA receptor subunit composition controls synaptic plasticity by regulating binding to CaMKII. *Neuron* 48, 289–301.
- Barrionuevo, G., and Brown, T.H. (1983). Associative long-term potentiation in hippocampal slices. *Proc. Natl. Acad. Sci. U S A* 80, 7347–7351.
- Branco, T., Staras, K., Darcy, K.J., and Goda, Y. (2008). Local dendritic activity sets release probability at hippocampal synapses. *Neuron* 59, 475–485.
- Chklovskii, D.B., Mel, B.W., and Svoboda, K. (2004). Cortical rewiring and information storage. *Nature* 431, 782–788.
- Costa-Mattioli, M., Sossin, W.S., Klann, E., and Sonnenberg, N. (2009). Translational control of long-lasting synaptic plasticity and memory. *Neuron* 61, 10–26.
- Desai, N.S., Cudmore, R.H., Nelson, S.B., and Turrigiano, G.G. (2002). Critical periods for experience-dependent synaptic scaling in visual cortex. *Nat. Neurosci.* 5, 783–789.
- Desai, N.S., Rutherford, L.C., and Turrigiano, G.G. (1999). Plasticity in the intrinsic excitability of cortical pyramidal neurons. *Nat. Neurosci.* 2, 515–520.
- Erdil, E., Yagci, A.M., Argunsah, A.O., Ramiro-Cortes, Y., Hobbiss, A.F., Israely, I., and Unay, D. (2012). A tool for automatic dendritic spine detection and analysis. Part I: dendritic spine detection using multi-level region-based segmentation. *3rd International Conference On Image Processing Theory, Tools and Applications, IPTA*, 167–171.
- Félix-Oliveira, A., Dias, R.B., Colino-Oliveira, M., Rombo, D.M., and Sebastião, A.M. (2014). Homeostatic plasticity induced by brief activity deprivation enhances long-term potentiation in the mature rat hippocampus. *J. Neurophysiol.* 112, 3012–3022.
- Fernandes, D., and Carvalho, A.L. (2016). Mechanisms of homeostatic plasticity in the excitatory synapse. *J. Neurochem.* 139, 973–996.
- Fu, M., Yu, X., Lu, J., and Zuo, Y. (2012). Repetitive motor learning induces coordinated formation of clustered dendritic spines *in vivo*. *Nature* 483, 92–95.
- Ghani, M.U., Mesadi, F., Kanık, S.D., Argunşah, A.Ö., Hobbiss, A.F., Israely, I., Ünay, D., Taşdizen, T., and Çetin, M. (2017). Dendritic spine classification using shape and appearance features based on two-photon microscopy. *J. Neurosci. Methods* 279, 13–21.

- Govindarajan, A., Israely, I., Huang, S.-Y.Y., and Tonegawa, S. (2011). The dendritic branch is the preferred integrative unit for protein synthesis-dependent LTP. *Neuron* 69, 132–146.
- Govindarajan, A., Kelleher, R.J., and Tonegawa, S. (2006). A clustered plasticity model of long-term memory engrams. *Nat. Rev. Neurosci.* 7, 575–583.
- Harvey, C.D., and Svoboda, K. (2007). Locally dynamic synaptic learning rules in pyramidal neuron dendrites. *Nature* 450, 1195–1200.
- Harvey, C.D., Yasuda, R., Zhong, H., and Svoboda, K. (2008). The spread of Ras activity triggered by activation of a single dendritic spine. *Science* 321, 136–140.
- Hu, J.-H., Park, J.M., Park, S., Xiao, B., Dehoff, M.H., Kim, S., Hayashi, T., Schwarz, M.K., Huganir, R.L., Seeburg, P.H., et al. (2010). Homeostatic scaling requires group I mGluR activation mediated by Homer1a. *Neuron* 68, 1128–1142.
- Huganir, R.L., and Nicoll, R.A. (2013). AMPARs and synaptic plasticity: the last 25 years. *Neuron* 80, 704–717.
- Ju, W., Morishita, W., Tsui, J., Gaietta, G., Deerinck, T.J., Adams, S.R., Garner, C.C., Tsien, R.Y., Ellisman, M.H., and Malenka, R.C. (2004). Activity-dependent regulation of dendritic synthesis and trafficking of AMPA receptors. *Nat. Neurosci.* 7, 244–253.
- Karmarkar, U.R., and Buonomano, D.V. (2006). Different forms of homeostatic plasticity are engaged with distinct temporal profiles. *Eur. J. Neurosci.* 23, 1575–1584.
- Keck, T., Keller, G.B., Jacobsen, R.I., Eysel, U.T., Bonhoeffer, T., and Hübener, M. (2013). Synaptic scaling and homeostatic plasticity in the mouse visual cortex *in vivo*. *Neuron* 80, 327–334.
- Kirov, S.A., and Harris, K.M. (1999). Dendrites are more spiny on mature hippocampal neurons when synapses are inactivated. *Nat. Neurosci.* 2, 878–883.
- Kleindienst, T., Winnubst, J., Roth-Alpermann, C., Bonhoeffer, T., and Lohmann, C. (2011). Activity-dependent clustering of functional synaptic inputs on developing hippocampal dendrites. *Neuron* 72, 1012–1024.
- Komiyama, N.H., Watabe, A.M., Carlisle, H.J., Porter, K., Charlesworth, P., Monti, J., Strathdee, D.J.C., O'Carroll, C.M., Martin, S.J., Morris, R.G.M., et al. (2002). SynGAP regulates ERK/MAPK signaling, synaptic plasticity, and learning in the complex with postsynaptic density 95 and NMDA receptor. *J. Neurosci.* 22, 9721–9732.
- Korte, M., Kang, H., Bonhoeffer, T., and Schuman, E. (1998). A role for BDNF in the late-phase of hippocampal long-term potentiation. *Neuropharmacology* 37, 553–559.
- Lee, M.-C., Yasuda, R., and Ehlers, M.D. (2010). Metaplasticity at single glutamatergic synapses. *Neuron* 66, 859–870.
- Liu, G. (2004). Local structural balance and functional interaction of excitatory and inhibitory synapses in hippocampal dendrites. *Nat. Neurosci.* 7, 373.
- Makino, H., and Malinow, R. (2011). Compartmentalized versus global synaptic plasticity on dendrites controlled by experience. *Neuron* 72, 1001–1011.
- Malenka, R.C., and Bear, M.F. (2004). LTP and LTD: an embarrassment of riches. *Neuron* 44, 5–21.
- Matsuzaki, M., Honkura, N., Ellis-Davies, G.C.R., and Kasai, H. (2004). Structural basis of long-term potentiation in single dendritic spines. *Nature* 429, 761–766.
- Murthy, V.N., Schikorski, T., Stevens, C.F., and Zhu, Y. (2001). Inactivity produces increases in neurotransmitter release and synapse size. *Neuron* 32, 673–682.
- O'Brien, R.J., Kamboj, S., Ehlers, M.D., Rosen, K.R., Fischbach, G.D., and Huganir, R.L. (1998). Activity-dependent modulation of synaptic AMPA receptor accumulation. *Neuron* 21, 1067–1078.
- Oh, W.C., Hill, T.C., and Zito, K. (2013). Synapse-specific and size-dependent mechanisms of spine structural plasticity accompanying synaptic weakening. *Proc. Natl. Acad. Sci. U.S.A.* 110, E305–E312.
- Oh, W.C.C., Parajuli, L.K.K., and Zito, K. (2015). Heterosynaptic structural plasticity on local dendritic segments of hippocampal CA1 neurons. *Cell Rep.* 10, 162–169.
- Paoletti, P., Bellone, C., and Zhou, Q. (2013). NMDA receptor subunit diversity: impact on receptor properties, synaptic plasticity and disease. *Nat. Rev. Neurosci.* 14, 383–400.
- Rabinowitch, I., and Segev, I. (2008). Two opposing plasticity mechanisms pulling a single synapse. *Trends Neurosci.* 31, 377–383.
- Ramiro-Cortés, Y., Hobbiss, A.F., and Israely, I. (2014). Synaptic competition in structural plasticity and cognitive function. *Philos. Trans. R. Soc. Lond. B Biol. Sci.* 369, 20130157.
- Ramiro-Cortés, Y., and Israely, I. (2013). Long lasting protein synthesis- and activity-dependent spine shrinkage and elimination after synaptic depression. *PLoS One* 8, e71155.
- Rutherford, L.C., Nelson, S.B., and Turrigiano, G.G. (1998). BDNF has opposite effects on the quantal amplitude of pyramidal neuron and interneuron excitatory synapses. *Neuron* 21, 521–530.
- Schanzenbacher, C.T., Langer, J.D., and Schuman, E.M. (2018). Time- and polarity-dependent proteomic changes associated with homeostatic scaling at central synapses. *Elife*, 1–20, <https://doi.org/10.7554/elife.33322>.
- Soares, C., Lee, K.F.H., and Béïque, J.-C. (2017). Metaplasticity at CA1 synapses by homeostatic control of presynaptic release dynamics. *Cell Rep.* 21, 1293–1303.
- Sutton, M.A., Ito, H.T., Cressy, P., Kempf, C., Woo, J.C., and Schuman, E.M. (2006). Miniature neurotransmission stabilizes synaptic function via tonic suppression of local dendritic protein synthesis. *Cell* 125, 785–799.
- Tang, S., and Yasuda, R. (2017). Imaging ERK and PKA activation in single dendritic spines during structural plasticity. *Neuron* 93, 1315–1324.e3.
- Thiagarajan, T.C., Lindskog, M., and Tsien, R.W. (2005). Adaptation to synaptic inactivity in hippocampal neurons. *Neuron* 47, 725–737.
- Toyoizumi, T., Kaneko, M., Stryker, M.P., and Miller, K.D. (2014). Modeling the dynamic interaction of hebbian and homeostatic plasticity. *Neuron* 84, 497–510.
- Turrigiano, G. (2011). Too many cooks? Intrinsic and synaptic homeostatic mechanisms in cortical circuit refinement. *Annu. Rev. Neurosci.* 34, 89–103.
- Turrigiano, G.G., Leslie, K.R., Desai, N.S., Rutherford, L.C., and Nelson, S.B. (1998). Activity-dependent scaling of quantal amplitude in neocortical neurons. *Nature* 391, 892–896.
- Vitureira, N., and Goda, Y. (2013). The interplay between hebbian and homeostatic synaptic plasticity. *J. Cell Biol.* 203, 175–186.
- Wallace, W., and Bear, M.F. (2004). A morphological correlate of synaptic scaling in visual cortex. *J. Neurosci.* 24, 6928–6938.
- Wang, C.C., Held, R.G., and Hall, B.J. (2013). SynGAP regulates protein synthesis and homeostatic synaptic plasticity in developing cortical networks. *PLoS One* 8, <https://doi.org/10.1371/journal.pone.0083941>.
- Yadav, A., Gao, Y.Z., Rodriguez, A., Dickstein, D.L., Wearne, S.L., Luebke, J.I., Hof, P.R., and Weaver, C.M. (2012). Morphologic evidence for spatially clustered spines in apical dendrites of monkey neocortical pyramidal cells. *J. Comp. Neurol.* 520, 2888–2902.
- Yee, A.X., Hsu, Y.-T., and Chen, L. (2017). A metaplasticity view of the interaction between homeostatic and Hebbian plasticity. *Philos. Trans. R. Soc. Lond. B Biol. Sci.* 372, 20160155.

Supplemental Information

**Homeostatic Plasticity Scales Dendritic
Spine Volumes and Changes the Threshold
and Specificity of Hebbian Plasticity**

Anna Felicity Hobbiss, Yazmin Ramiro-Cortés, and Inbal Israely

Figure S1 (related to Figure 1)

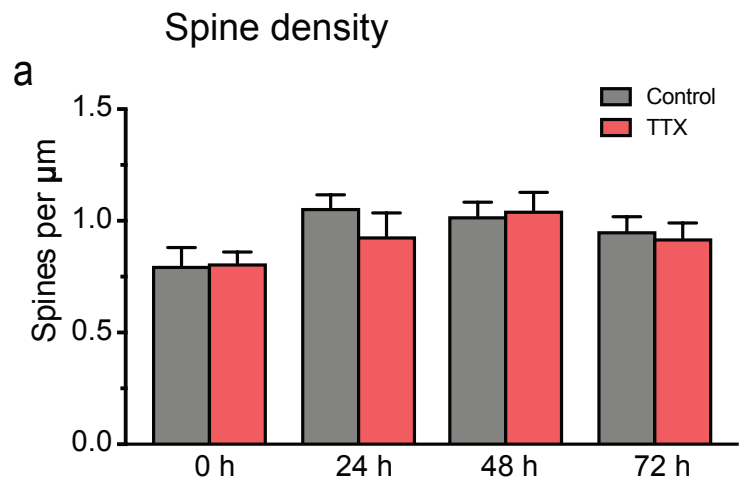


Figure S2 (related to Figure 1 and Figure 3)

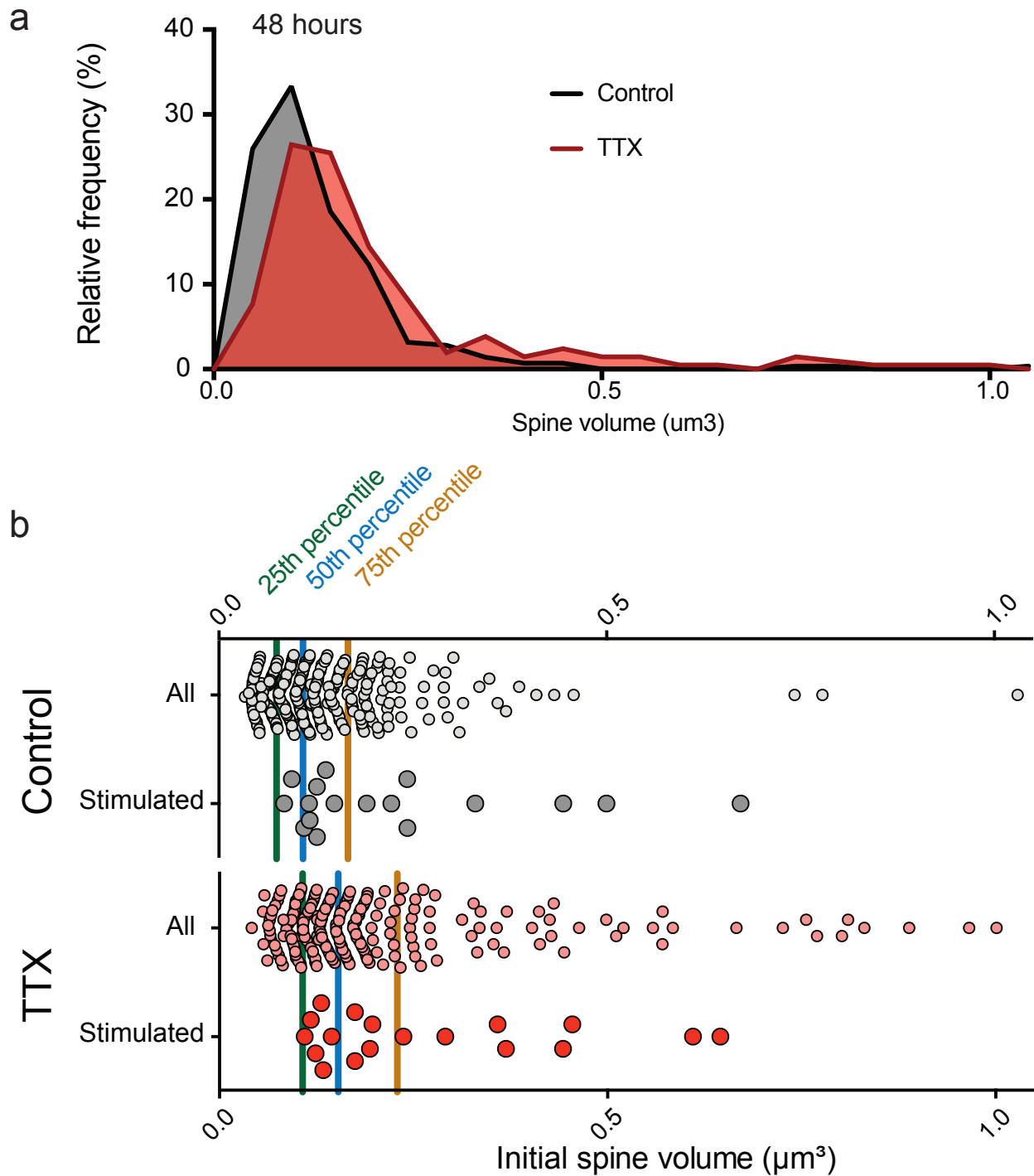
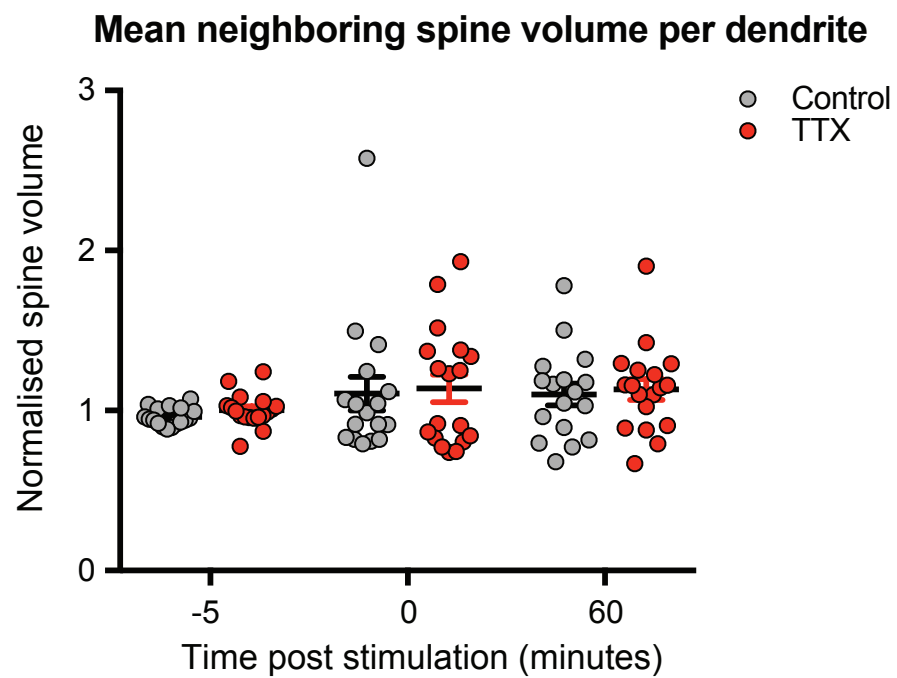


Figure S3 (related to Figure 5)



Supplemental Figure Legends

Figure S1 (related to Figure 1). Dendrite parameters after HSP

a) Spine density over 72 hours of activity blockade. N (dendrites) for the 0 h, 24 h, 48 h and 72 h timepoints: Control = 6,8,7,5. TTX = 7, 5, 6, 6. $p = 0.57$ for the effect of TTX on spine density over the timecourse (2-way ANOVA). ASM104xUSB3

Figure S2 (related to Figure 3). Population data for spine sizes following HSP

a) Histograms of pooled spine volumes at the 48 h timepoint. This is the same data as is presented in Figure 1f. b) Initial volumes (pre-stimulation) of the spines that underwent glutamate uncaging (same spines as presented in Figures 3c-h & Figure 4b-e, shown in comparison to the pooled spine populations 48 hours as shown in Figure S2a and Figure 1F. The 25th, 50th and 75th percentiles of the population data are indicated for each respective population.

Figure S3 (related to Figure 5). Spine size per dendrite following glutamate uncaging

a) Neighboring spines analysed in Figure 5 were grouped per dendrite and averaged. Points displayed are each individual dendrite mean. $p_{control-ttx} = 0.573$, 2-way ANOVA.

Transparent methods

Ethics Statement

All animal experiments were carried out in accordance with European Union regulations on animal care and use, and with the approval of the Champalimaud Centre for the Unknown Ethics Committee and the Portuguese Veterinary Authority (DGAV).

Slice culture preparation and biolistic transfection

Mouse hippocampal organotypic slice cultures were prepared using p7-10 C57BL/6J mice as previously described (Govindarajan, Israely, Huang, & Tonegawa, 2011). Briefly, hippocampi were dissected and 350 µm slices were cut with a tissue chopper in ice-cold artificial cerebral spinal fluid (aCSF) containing 2.5 mM KCl, 26 mM NaHCO₃, 1.15 mM NaH₂PO₄, 11 mM D-glucose, 24 mM sucrose, 1 mM CaCl₂ and 5 mM MgCl₂. The slices were cultured on membranes (Millipore), and maintained at an interface with the following media: 1x MEM (Invitrogen), 20% horse serum (Invitrogen), 1 mM GlutaMAX (Invitrogen), 27 mM D-glucose, 30 mM HEPES, 6 mM NaHCO₃, 2 mM CaCl₂, 2 mM MgSO₄, 1.2% ascorbic acid, 1 µg/ml insulin. The pH was adjusted to 7.3, and the osmolarity adjusted to 300–310 mOsm. All chemicals were from Sigma unless otherwise indicated. Media was changed every 2-3 days.

Biolistic transfection of slice cultures was accomplished using a Helios gene gun (Bio-Rad) after 4–7 days in vitro (DIV). Gold beads (10 mg, 1.6 µm diameter, Bio-Rad) were coated with 100 ng AFP-plasmid DNA (a GFP-expressing plasmid driven by the β-actin promoter (Inouye, Ogawa, Yasuda, Umesono, & Tsuji, 1997) according to the manufacturer's protocol and delivered biolistically to the slices, using a pressure of 160-180 psi.

Homeostatic plasticity induction by activity block

TTX (1 µM) was added to the culture media at 7-9 DIV. The day of application was then designated day 0 for experiments. Control experiments were maintained in normal culture media, and were age- and animal-matched to treated slices for experiments.

Electrophysiology

Hippocampal slice cultures were perfused continuously with aCSF (as above, with the addition of 0.5 µM TTX for all mEPSC recordings) for a pre-incubation period of 15 to 30 min. Whole cell voltage-clamp recordings were performed in CA1 pyramidal neurons, using 7–8 MΩ

electrodes. For mEPSC recordings, the internal solution contained 135 mM Cs-methanesulfonate, 10 mM CsCl, 10 mM HEPES, 5 mM EGTA, 2 mM MgCl₂, 4 mM Na-ATP and 0.1 mM Na-GTP, with the pH adjusted to 7.2 with KOH, at 290-295 mOsm. Cells were voltage clamped at -65 mV. Cellular recordings in which series resistance was higher than 25 mV were discarded. Stability was assessed throughout the experiment, with cells whose series resistance changed more than 30% being discarded. mEPSCs recordings were started 3 minutes after break-in and continued for 10 minutes. Signals were acquired using a Multiclamp 700B amplifier (Molecular Devices), and data was digitized with a Digidata 1440 at 3 kHz. mEPSC events were detected off-line using Mini-Analysis Program (Synaptosoft). Events smaller than 15 pA fell within the range of noise in the system and were not included in the analysis. For spontaneous activity recordings, slices were perfused continuously with aCSF without the addition of TTX for a pre-incubation period of 5 to 10 min. The internal solution for the electrodes contained 136.5 mM K-Gluconate, 9 mM NaCl, 17.5 mM KCl, 10 mM HEPES, 0.2 mM EGTA, and 0.025 mM Alexa 594, with the pH adjusted to 7.2 with KOH, at 280-290 mOsm. In current clamp with no external current applied, an IV curve was first recorded to check for spike frequency accommodation in order to validate the identity of pyramidal neurons. Spiking events were then recorded for a period of 6-9 minutes. The addition of Alexa-594 allowed cells to be imaged post-recording.

Two-photon Imaging

Two-photon imaging was performed on a BX61WI Olympus microscope, using a galvanometer-based scanning system (Prairie Technologies /Bruker) with a Ti:sapphire laser (910 nm for imaging AFP; Coherent), controlled by PrairieView software (Prairie Technologies). Slices were perfused with oxygenated aCSF containing 127 mM NaCl, 2.5 mM KCl, 25 mM NaHCO₃, 1.25 mM NaH₂PO₄, 25 mM D-glucose, 2 mM CaCl₂, 1 mM MgCl₂ and 0.5 μM TTX (equilibrated with O₂ 95%/CO₂ 5%) at room temperature, at a rate of 1.5 ml/min. Secondary or tertiary apical dendrites of CA1 neurons (where the apical trunk is counted as the primary branch) were imaged using a water immersion objective (60x, 1.0 NA, Olympus LUMPlan FLN) with a digital zoom of 8x. For each neuron, 2-3 dendrites were imaged. Z-stacks (0.5 μm per section) were collected at a resolution of 1024 x 1024 pixels, resulting in a field of view of 25.35 x 25.35 μm. 3 images were taken per dendrite at 5-minute intervals, with the reported spine volume being the average of the 3 images. Images were taken at the highest

possible fluorescence intensity without image saturation in order to accurately quantify spine volumes (see below).

Glutamate uncaging

Uncaging experiments (Pettit, Wang, Gee, & Augustine, 1997) and caged glutamate calibration were carried out as previously described (Govindarajan et al., 2011), and briefly as follows. MNI-caged-L-glutamate (MNI-Glu) (Tocris) was reconstituted in the dark in aCSF lacking MgCl₂ or CaCl₂ to make a 10 mM stock solution. Individual aliquots were diluted to the working concentration of 2.5 mM MNI-Glu in uncaging aCSF (see below), in 3 ml volumes. We tested each batch of reconstituted MNI-Glu as previously described (Govindarajan et al., 2011). Briefly, five uncaging test pulses of 1 ms were delivered to single spines and evoked EPSCs were measured by whole cell patch clamp recordings. We compared these to spontaneous mEPSCs, and determined the power needed (60mW at the back aperture) to produce an uncaging EPSC of comparable size to that of an average spontaneous mEPSC. During plasticity experiments, slices were incubated for 30-45 minutes in normal aCSF as described above. Uncaging was performed using a Ti:sapphire laser (720 nm; Coherent), controlled by PrairieView software (Prairie Technologies, Bruker). All stimuli were carried out in uncaging-aCSF containing: 2.5 mM MNI-Glu, 0 mM MgCl₂, and 4 mM CaCl₂. The uncaging train consisted of 30 pulses at 0.5 Hz, with a pulse width of either 4 ms (standard protocol) or 1 ms (sub-threshold protocol), using 30mW power as measured at the back aperture (half the power as determined in the calibration step, as previously described for an uncaging LTP protocol (Govindarajan et al., 2011)). The uncaging point was positioned 0.6 µm from the end of the spine head, away from the parent dendrite. Each experiment began with a sham stimulation in uncaging-aCSF lacking MNI-Glu on a control dendrite of the experimental neuron, to rule out the possibility of non-specific structural changes due to phototoxicity or poor neuronal health. Subsequently, experimental spines on new dendrites were identified, uncaging-aCSF containing 2.5mM MNI-glutamate was recirculated for 5 minutes, and the uncaging protocol was delivered. Fast imaging (approximately 20 Hz) of a region of interest (ROI) of the stimulated spine head and neck was performed throughout the 60 second stimulation, to record the growth dynamics for this time period. After the stimulation, the perfusion was returned to normal aCSF for the remainder of the experiment (1-2 hours). The

first image was taken immediately after returning to normal aCSF and is designated as time = 0 post stimulation.

Spine Volume Determination

To quantify spine volume, we used the custom built Matlab plug-in SpineS, which uses semi-automatic detection, automatic alignment and segmentation of spine heads (Ghani et al., 2017). Spine volume was calculated using the summed fluorescence intensity of the spine, normalized to the median fluorescence intensity of the parent dendrite, in order to correct for changes in overall fluorescence levels within a cell. Fluorescence intensity was converted to real volumes by taking Full Width Half Max (FWHM) measurements of spines and calculating a conversion factor between the two measures (Matsuzaki, Honkura, Ellis-Davies, & Kasai, 2004). For the homeostatic plasticity analysis (Figures 1 & 2), all spines with a discernible head within the field of view were included in the analysis, unless obstructed by other structures. For the uncaging analysis (Figures 3, 4 & 5), between 2 and 8 neighboring spines were analyzed from the same dendrite, within the whole field of view. Neighboring spines were located between 0.1 μm to 22 μm from the stimulated spine, with a mean distance of 9.0 μm . Normalization of spine volumes throughout the experiment was performed using the mean of three baseline images.

Statistical analyses

All statistical analyses were carried out in Graphpad Prism. Stars (*) represent degrees of significance as follows: (*) = $p < 0.05$; (**) = $p < 0.01$; (***) = $p < 0.001$). Unless otherwise specified, all tests were 2-tailed.

SUPPLEMENTAL REFERENCES

- Ghani, M. U., Mesadi, F., Kanik, S. D., Argunsah, A. O., Hobbiss, A. F., Israely, I., ... Cetin, M. (2017). Dendritic spine classification using shape and appearance features based on two-photon microscopy. *Journal of Neuroscience Methods*, 279, 13–21.
<https://doi.org/https://doi.org/10.1016/j.jneumeth.2016.12.006>
- Govindarajan, A., Israely, I., Huang, S.-Y., & Tonegawa, S. (2011). The dendritic branch is the preferred integrative unit for protein synthesis-dependent LTP. *Neuron*, 69(1), 132–146. <https://doi.org/10.1016/j.neuron.2010.12.008>
- Inouye, S., Ogawa, H., Yasuda, K., Umesono, K., & Tsuji, F. I. (1997). A bacterial cloning vector using a mutated Aequorea green fluorescent protein as an indicator. *Gene*, 189(2), 159–162. [https://doi.org/10.1016/S0378-1119\(96\)00753-6](https://doi.org/10.1016/S0378-1119(96)00753-6)
- Matsuzaki, M., Honkura, N., Ellis-Davies, G. C. R., & Kasai, H. (2004). Structural basis of long-term potentiation in single dendritic spines. *Nature*, 429(June), 761–766.
<https://doi.org/10.1038/nature02594.1>
- Pettit, D. L., Wang, S. S. H., Gee, K. R., & Augustine, G. J. (1997). Chemical two-photon uncaging: A novel approach to mapping glutamate receptors. *Neuron*, 19(3), 465–471.
[https://doi.org/10.1016/S0896-6273\(00\)80361-X](https://doi.org/10.1016/S0896-6273(00)80361-X)